© 2015. Published by The Company of Biologists Ltd | Journal of Cell Science (2015) 128, 4160-4170 doi:10.1242/jcs.172395

RESEARCH ARTICLE

A microtubule-independent role of p150^{glued} in secretory cargo concentration at endoplasmic reticulum exit sites

Fatima Verissimo[1], Aliaksandr Halavatyi[1], Rainer Pepperkok[1,*] and Matthias Weiss[2,*]

ABSTRACT

Newly synthesized proteins are sorted into COPII-coated transport carriers at the endoplasmic reticulum (ER). Assembly of the COPII coat complex, which occurs at ER exit sites (ERES), is initiated by membrane association and GTP loading of SAR1, followed by the recruitment of the SEC23–SEC24 and SEC13–SEC31 subcomplexes. Both of these two subcomplexes stimulate GTP hydrolysis and coat disassembly. This inherent disassembly capacity of COPII complexes needs to be regulated to allow sufficient time for cargo sorting and transport carrier formation. By performing fluorescence recovery after photobleaching (FRAP) and mathematical modeling, we show that p150^{glued} (also known as DCTN1), a component of the dynactin complex, stabilizes the COPII pre-budding complex on ER membranes in a microtubule-independent manner. Concentration of the secretory marker ts-O45-G at ERES is reduced in the presence of a C-terminal p150^{glued} fragment that prevents binding of endogenous p150^{glued} to SEC23. A similar cargo reduction is observed upon p150^{glued} knockdown. Taken together, our data suggest that cargo concentration at ERES is regulated by p150^{glued} to coordinate protein sorting and transport carrier formation with the subsequent long-range transport towards the Golgi complex along microtubules.

KEY WORDS: Endoplasmic reticulum, ER exit sites, Protein sorting, Microtubules, Secretory pathway, FRAP, Modeling

INTRODUCTION

Biosynthetic cargo is sorted at the endoplasmic reticulum (ER) into COPII-coated transport carriers that mediate transport from the ER towards the Golgi (Barlowe, 2002; Otte and Barlowe, 2004). Formation of COPII vesicles *in vitro* requires only the minimal machinery, consisting of three components (Lee et al., 2004; Matsuoka et al., 1998). The COPII coat complex assembly is initiated by GTP loading of the small GTPase SAR1, leading to its firm association with membranes. Subsequently, membrane-bound SAR1 recruits the SEC23–SEC24 and SEC13–SEC31 subcomplexes, which leads to the formation of COPII-coated vesicles. Interestingly, binding of SEC23–SEC24 and SEC13–SEC31 subcomplexes stimulate GTP hydrolysis by SAR1 (Antonny et al., 2001) inducing coat disassembly. This intrinsic disassembly capacity of the COPII complex suggests that it is metastable and raises the question of how cargo sorting can be achieved before the COPII coat disassembles. In analogy to clathrin coat assembly regulation (Hehnly and Stamnes, 2007; Slepnev and De Camilli, 2000), it is tempting to hypothesize that additional accessory proteins might interact with the COPII proteins to regulate its membrane association and dissociation, and COPII carrier formation.

In support of this hypothesis secretory cargo prevents premature COPII disassembly by stabilizing the COPII complex after GTP hydrolysis (Forster et al., 2006; Sato and Nakano, 2005). Turnover of SEC23 at ERES has also been shown to change upon depletion of cellular sterols (Runz et al., 2006). This indicates that several factors, including lipids, might act in concert to regulate the turnover of COPII complexes on ER membranes. Along these lines, PCTAIRE protein kinases and signal-transducing adaptor molecules (STAMs) have been shown to interact with the COPII complex and to modulate secretory cargo transport (Palmer et al., 2005; Rismanchi et al., 2009). p150^{glued} (also known as DCTN1), a component of the dynactin complex that enhances motor processivity (Culver-Hanlon et al., 2006; King and Schroer, 2000) and binding of dynein motors to microtubules (Waterman-Storer et al., 1995), directly interacts with the COPII pre-budding complex (SAR1–SEC23–SEC24) (Watson et al., 2005). Interfering with the interaction of p150^{glued} and the COPII pre-budding complex leads to an inhibition of ER-to-Golgi transport of secretory cargo, but has no apparent effect on the motility of ER-to-Golgi transport carriers (Watson et al., 2005).

To understand the role of p150^{glued} on COPII carrier formation and cargo transport, here, we used fluorescence recovery after photobleaching (FRAP) to quantitatively determine the turnover of the individual COPII subunits SAR1, SEC23 and SEC31 at single ER exit sites (ERES) in stably transfected cells. We found that COPII turnover kinetics at single ERES is changed in the presence of a C-terminal p150^{glued} fragment (CT^{glued}) that inhibits binding of endogenous p150^{glued} to SEC23. Thereafter, we applied mathematical modeling to determine which substeps of COPII turnover at ERES are affected by CT^{glued} using our FRAP data and measurements of the associated ERES-bound steady-state fraction of COPII proteins. This analysis predicted that the interaction of SEC23 with p150^{glued} is required to stabilize the COPII pre-budding complex. Consistent with this prediction, we observed that inhibiting the SEC23–p150^{glued} interaction with the antagonistic CT^{glued} or downregulating p150^{glued} with chemically synthesized small interfering RNAs (siRNAs) prevented the concentration of the secretory cargo ts-O45-G (Zilberstein et al., 1980) at ERES in a microtubule-independent manner. Taken together, our data suggest that cargo concentration at ERES is enhanced by the SEC23–p150^{glued} interaction, providing a mechanism to coordinate the formation of transport intermediates with their subsequent long-range transport towards the Golgi complex along microtubules.

[1]Cell Biology and Biophysics Unit, EMBL, Meyerhofstraße 1, Heidelberg D-69117, Germany. [2]Experimental Physics I, Universitaetsstr. 30, University of Bayreuth, Bayreuth D-95440, Germany.

*Authors for correspondence (matthias.weiss@uni-bayreuth.de; pepperko@embl-heidelberg.de)

Received 30 March 2015; Accepted 5 October 2015

Journal of Cell Science (2015) 128, 4160-4170 doi:10.1242/jcs.172395

RESULTS

Overexpression of the C-terminal fragment of p150^{glued} affects COPII turnover kinetics

To study the role of p150^{glued} on COPII membrane turnover we used FRAP on single ERES. Going beyond our previous approach (Watson et al., 2005), the membrane turnover of YFP-tagged versions of SAR1, SEC23 or SEC31 (the SAR1A, SEC23A and SEC31A isoforms) was quantified in stably expressing HeLa cells (Fig. 1 and Materials and Methods). FRAP data were complemented with measurements of the ERES-associated steady-state fraction of these COPII components. In unperturbed control cells, we observed a mean half-time for recovery ($t_{1/2}$) of 1.28 s±0.09 s for SAR1, whereas SEC23 showed markedly slower recovery kinetics ($t_{1/2}$=3.37 s±0.31 s) consistent with our earlier work (see Table 1 and Forster et al., 2006). The half-time determined for SEC31 ($t_{1/2}$=1.16 s±0.06 s) was similar to that obtained for SAR1 (Table 1) and faster than in our previous work (Watson et al., 2005) that employed a different SEC31 splice variant (Fig. S1A,B). In fact, an altered SEC31 turnover might be a combined consequence of different cell types (HeLa versus Vero), the form of transfection (stable versus transient), and different splice variants. To probe whether the YFP–SEC31 variant used in this study was functional and capable of supporting vital functions of the COPII coat, we tested whether the construct was able to replace endogenous SEC31 regarding ERES morphology and function. To this end, endogenous SEC31 was knocked down by RNA interference leading to a clear reduction of ERES labeling with SEC13 (see Fig. S1C). Subsequent expression of YFP-tagged SEC31, but not YFP alone, resulted in a recovery of normal ERES (Fig. S1D). This observation strongly suggests that the YFP-tagged SEC31 splice variant used here can substitute for the endogenous SEC31.

To elucidate the effect of p150^{glued} in the regulation of the COPII coat turnover, a previously characterized C-terminal fragment of p150^{glued} (amino acids 938–1254, here called CT^{glued}) was used (Watson et al., 2005). This fragment acts as an antagonist of p150^{glued} by directly interacting with SEC23 and competing with the endogenous p150^{glued} without causing the dissociation of the dynactin complex (Watson et al., 2005). In cells expressing CT^{glued}, the turnover kinetics for SAR1 remained largely unchanged (Table 1). However, perturbing the p150^{glued}–SEC23 interaction clearly affected the turnover of SEC23 and SEC31 (Table 1). Notably, the ERES-bound steady-state protein fraction did not change substantially compared to control cells for all tested COPII subunits.

Having observed substantial changes in the turnover times of SEC23 and SEC31, we wondered which steps in COPII (dis) assembly might be involved here. Given that a single ERES is a small target region, our FRAP times only report on average dissociation rates of COPII proteins (see Hoffmann et al., 2015, for a discussion) without dissecting specific substeps. Yet, at least SEC23 might exist in multiple states that all contribute to this averaged dissociation rate: it might be part of the pre-budding complex SAR1–SEC23–SEC24 or of the fully developed COPII complex SAR1–SEC23–SEC24–SEC13–SEC31, and both complexes might even have substates depending on the presence of SAR1 and/or cargo (Forster et al., 2006). Given that a simple two-state binding–unbinding model for each COPII component is not sufficient to gain deeper mechanistic insights upon which one can derive experimentally testable predictions, we developed a more elaborate model for this purpose.

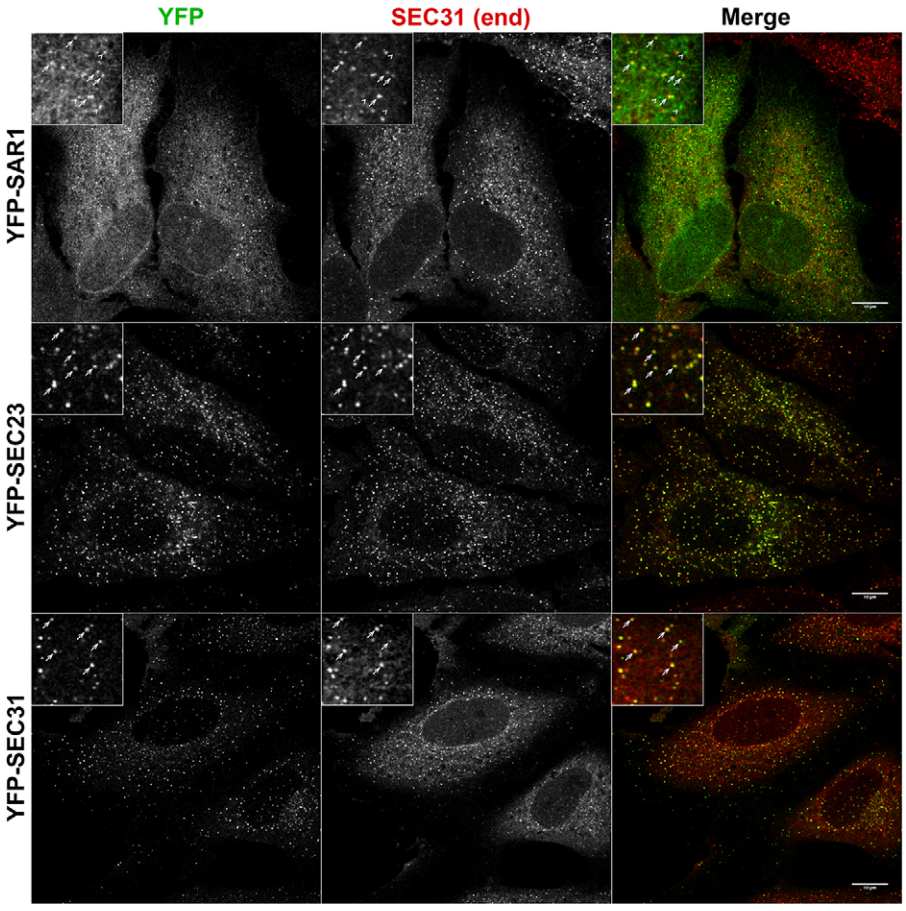

Fig. 1. Colocalization of stably expressed and endogenous ERES markers. Stable HeLa Kyoto cell lines expressing YFP–SAR1 (top panels), YFP–SEC23 (middle panels) and YFP–SEC31 (bottom panels) (green) colocalize with the endogenous COPII marker SEC31 (red) as seen in the merged images. Enlarged regions shown in the upper left corner highlight the colocalization with the endogenous SEC31 (arrows); ERES that did not show colocalization are highlighted with arrowheads. Scale bars: 10 µm.

Journal of Cell Science (2015) 128, 4160-4170 doi:10.1242/jcs.172395

Table 1. ERES-bound fraction of YFP-tagged COPII subunits and turnover kinetics at single ERES in the absence or presence of CT^{glued}

YFP–COPII subunit	CT^{glued}	$t_{1/2}$ (s)†	ERES fraction*,†
SAR1	–	1.28±0.09	0.23±0.02
SAR1	+	1.32±0.02	0.34±0.04
SEC23	–	3.37±0.31	0.40±0.03
SEC23	+	1.58±0.26	0.42±0.03
SEC31	–	1.16±0.06	0.24±0.01
SEC31	+	2.44±0.34	0.20±0.02

*Total fluorescence of YFP-tagged COPII subunit associated with ERES divided by the total fluorescence in the cell.
†Results are mean±s.e.m. of at least 20 cells per condition.

Uncovering the action of the C-terminal fragment of p150^{glued} using a kinetic model

Given that COPII coat assembly and disassembly is somewhat more complex than an elementary association–dissociation cycle of a single protein, our experimental FRAP results do not provide immediate information on individual substeps of COPII turnover at ERES. To overcome this limitation, we have previously developed a simple kinetic model that quantitatively describes the assembly and membrane turnover of COPII components at ERES in living cells (Forster et al., 2006). By adjusting the kinetic parameters of this model to reproduce the experimental FRAP data, we were able to make experimentally testable predictions on the role of cargo on turnover of COPII (Forster et al., 2006). In this model, however, the turnover of the SEC23–SEC24 and SEC13–SEC31 subcomplexes at ERES had been assumed to occur coincidently and not sequentially. However, as p150^{glued} interacts with the pre-budding complex (SAR1–SEC23–SEC24), but not with the SEC13–SEC31 subcomplex (Watson et al., 2005), this model is somewhat too simple to properly reveal the action of p150^{glued} on COPII.

Therefore, we developed a new and more elaborate kinetic model of COPII membrane turnover that considers both subcomplexes separately (Fig. 2A and see the Materials and Methods for details of the model). This model was designed in such a way that each of the individual reaction steps is consistent with *in vitro* data on COPII complex assembly and disassembly, membrane association and COPII vesicle biogenesis in the literature (see, for example, Antonny et al., 2001; Lee et al., 2004). In our model (Fig. 2A) the GDP-bound form of SAR1 is recruited to ERES in an inactive form with rate *k*. At this point, SAR1 can either dissociate again (rate Γ) or undergo nucleotide exchange, which leads to a firm association of SAR1 with ER membranes. The GTP-bound form of SAR1 subsequently recruits the subcomplex SEC23–SEC24 (rate ω), which stimulates GTP hydrolysis (Antonny et al., 2001) and, hence, can trigger the sequential release of SAR1 (rate γ_1) and SEC23–SEC24 (rate λ_1) from ERES. The pre-budding complex SAR1–SEC23–SEC24 is known to be required for the binding of the outer layer of the COPII complex, the SEC13–SEC31 subcomplex (Antonny et al., 2001; Matsuoka et al., 1998; Stagg et al., 2008), a step which finally leads to COPII vesicle budding. In our model, binding of SEC13–SEC31 to the pre-budding complex SAR1–SEC23–SEC24 occurs with rate β. The fully assembled COPII coat can subsequently disassemble in a sequential manner. First, upon hydrolysis of GTP, an event that is further stimulated by SEC13–SEC31 binding (Antonny et al., 2001), SAR1 is released from the membrane with rate γ_2. Subsequently, the SEC23–SEC24–SEC13–SEC31 complex is released with rate λ_2. Formulating this kinetic reaction network in mathematical terms, we were able to calculate the ERES-bound steady-state fractions of COPII components and FRAP curves for arbitrary parameter sets (see Materials and Methods). Comparing these *in silico* data with experimental data allowed us to identify parameter sets of the model that led to steady states and FRAP curves that are consistent with our

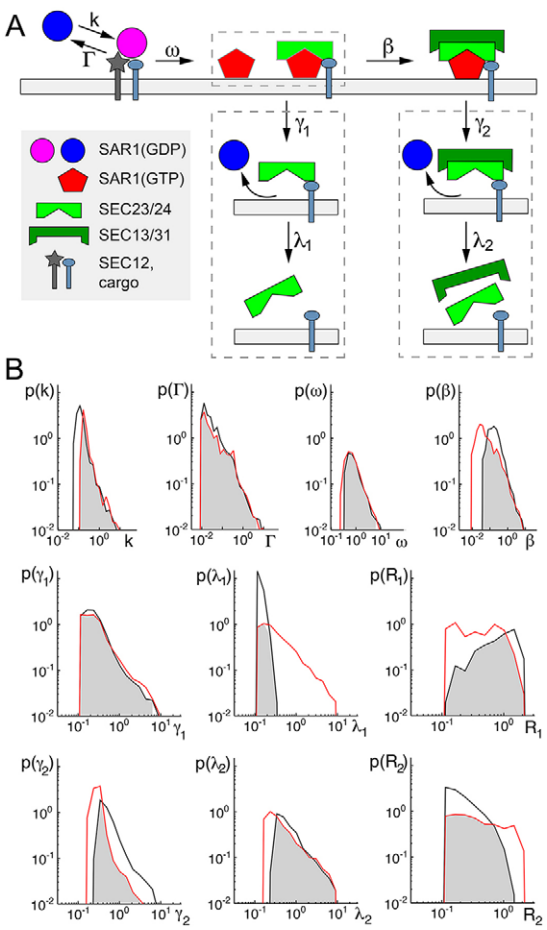

Fig. 2. Kinetic model of COPII protein turnover at single ERES. (A) In line with our earlier model (Forster et al., 2006) we assumed that SAR1 binds to ERES through association with SEC12 and/or cytoplasmic tails of cargo proteins (rate k). Dissociation (without nucleotide exchange) might occur with rate Γ. Alternatively, SAR1 undergoes nucleotide exchange and rapidly recruits SEC23–SEC24 (SEC23/24). As both events have been shown to happen almost concomitantly (Antonny et al., 2001), we combined them into a single step with rate ω. Upon GTP hydrolysis SAR1 is released (rate γ_1), while the rest of the pre-budding complex remains associated with the membrane and detaches subsequently with rate λ_1. Alternatively, the SAR1–SEC23–SEC24 complex can recruit SEC13–SEC31 (SEC13/31) (rate β). In analogy to the pre-budding complex, the full COPII complex can dissociate sequentially with rates γ_2 (SAR1 release after GTP hydrolysis) and λ_2 (coat dissociation). The kinetic scheme thus relies on eight kinetic rate constants and two parameters describing the relative cellular expression levels of COPII components, R_1=[SEC23]/[SAR1] and R_2=[SEC31]/[SAR1]. See Materials and Methods for mathematical details. (B) By randomly screening model parameters, we identified 2000 parameter sets that yielded good fits of the model to our experimental data with and without CT^{glued} (see Materials and Methods for details). Given that individual parameter values varied considerably, we used the probability distributions of the parameters to highlight which steps of COPII (dis)assembly are most affected by the expression of CT^{glued}. Black and red lines denote the distribution of the parameters found by comparing the model to untreated and CT^{glued}-treated cells, respectively. The geometric mean of each distribution and the percentage overlap between the two distributions (gray-shaded region) are listed in Table 2. As a primary result, the model predicts an enhanced disassembly rate of the pre-budding complex (λ_1) upon CT^{glued} expression and, to a lesser extent, a slowed-down release of the full coat complex (γ_2). See main text and Table 2 for more details.

Journal of Cell Science (2015) 128, 4160-4170 doi:10.1242/jcs.172395

Table 2. Geometric averages of model parameters in the absence or presence of CT^{glued}, and overlaps of parameters distributions for both conditions

Parameter	Without CT^{glued}	With CT^{glued}	Ratio (with CT^{glued}): (without CT^{glued})	Distribution overlap
k [1/s]	0.57	1.52	2.67	65%
Γ [1/s]	4.83	7.30	1.51	89%
ω [1/s]	6.87	4.95	0.72	91%
γ_1 [1/s]	0.57	0.70	1.23	90%
λ_1 [1/s]	0.14	1.10	7.86*	15%
β [1/s]	0.61	3.89	6.38	60%
γ_2 [1/s]	0.84	0.39	0.46*	43%
λ_2 [1/s]	1.40	1.31	0.94	83%
R_1	1.12	0.64	0.57	59%
R_2	0.30	0.75	2.3	53%

experiments (with and without CT^{glued}). It is worth noting at this point that the entire reaction network needs to be taken into account even if only individual COPII proteins are probed by performing FRAP in each experiment because the association–dissociation process (and hence the FRAP times) also includes these 'hidden' states.

To avoid a biased parameter search, we performed a random screen for parameter sets that yield an agreement between model and experimental data for each of the two experimental conditions, untreated and CT^{glued}-expressing cells (see Materials and Methods). For both conditions, we screened until we had found 2000 of such 'valid' parameter sets. Given that the values found for individual parameters showed a considerable variation, we determined the probability distributions for each parameter and condition (Fig. 2B) to identify the steps of COPII (dis)assembly affected by $p150^{glued}$. Indeed, most parameters showed a fairly broad distribution for both conditions, i.e. drawing conclusions solely on the basis of arithmetically averaged parameter values appeared inadequate. The observed variation in parameter values could indicate that our model is somewhat underdetermined, i.e. there are not enough experimental constraints to narrow down all rates to a small range of values. However, ubiquitous cell-to-cell variations imply that a model that can only describe experimental observations with a narrow range of parameters would not be robust enough to describe living systems (see, for example, Barkai and Leibler, 1997, for a discussion). The observation that our model can yield similar COPII turnover kinetics at ERES for a broad distribution of parameters therefore rather underlines the robustness of the reaction scheme shown in Fig. 2A.

To evaluate the set of 'valid' model parameters, we employed the geometric mean of each parameter value (Table 2). Unlike arithmetic averaging, taking a geometric mean relies on averaging on a logarithmic scale and is, hence, better suited to describe data with a broad distribution. In addition, the overlap of the probability distributions found for control and CT^{glued}-expressing cells was used to evaluate whether or not a change in the parameter was considered substantial (see also Materials and Methods and Fig. 2B for definition). Changes were considered substantial when this overlap was lower than 50% (see Table 2). This approach revealed that upon expression of CT^{glued}, only two rates changed substantially: the dissociation rate of the pre-budding complex without SAR1 (λ_1) was strongly altered and the dissociation rate of SAR1 from the mature COPII complex (γ_2) was affected to a lower extent. Our model therefore suggests that CT^{glued} primarily induces an increased dissociation rate of the pre-budding complex (λ_1) resulting in a shortened residence time of the pre-budding complex on ERES, whereas the SEC23-containing full COPII complex is much less affected. In support of this notion, the steady-state solution of the model for the mean parameter values in Table 2 revealed that the amount of SEC23–SEC24 in the pre-budding complex versus the total amount of membrane-bound SEC23–SEC24 decreased in the presence of CT^{glued} (see Materials and Methods for the calculation): whereas the fraction of SEC23–SEC24 in the pre-budding complex was 83% in untreated cells, a strong reduction to 28% emerged in the presence of CT^{glued}.

Based on our measurements of COPII kinetics and ERES steady states, the model suggests a reduced lifetime of the pre-budding complex as a major consequence of the presence of CT^{glued}. As the role of the pre-budding complex involves cargo capture and sorting (Aridor et al., 1998), we therefore hypothesized that a less stable pre-budding complex in CT^{glued}-expressing cells would result in a lower concentration of secretory cargo at ERES. An experimental verification of this prediction would indicate a clear role of $p150^{glued}$ in stabilizing the pre-budding coat, hence assuring cargo concentration at ERES.

Expressing the C-terminal fragment of $p150^{glued}$ reduces cargo concentration at ERES

To experimentally test the prediction of the model that in the presence of CT^{glued} secretory cargo concentration is reduced at ERES, we monitored by time-lapse microscopy the concentration of ts-O45-G into ER-derived transport carriers. Ts-O45-G is a well-established secretory cargo marker (Zilberstein et al., 1980). It accumulates in the ER at 39.5°C and is transported via the Golgi complex to the plasma membrane at the permissive temperature of 32°C. As expected, in our experiment, ts-O45-G accumulated in discrete structures at the ER when the temperature was shifted from 39.5°C to 32°C (Fig. 3A–C; Movies 1 and 2). The intensities of these structures increased gradually over time before the structures segregated from the ER and moved towards the Golgi complex (Fig. 3B; see also Presley et al., 1997; Runz et al., 2006; Scales et al., 1997 and Movies 1 and 2). The time between the first appearance of these structures and their release from the ERES varied considerably, from a few seconds to several minutes (data not shown). On average a maximum increase in fluorescence in these structures by factor 3.20±0.12 (mean±s.e.m., n=144) relative to neighboring ER membranes could be determined in control cells (Fig. 3D). In accordance with our model predictions, the concentration of the cargo marker ts-O45-G at ERES was reduced (to 1.70±0.05) in cells expressing CT^{glued} (Fig. 3D). Consistent with earlier work, the movement of these structures en route to the Golgi complex depended on microtubules (see also Movie 3), and the speed of movement was comparable between control cells and those expressing CT^{glued} (Watson et al., 2005 and data not shown).

To confirm that the reduction of cargo concentration at ERES upon expression of CT^{glued} was due to the deficit of fully functional $p150^{glued}$ at ERES, we performed a knockdown of the endogenous $p150^{glued}$ and measured the accumulation of the secretory marker ts-O45-G at ERES. In our experimental conditions, the knockdown efficiency of $p150^{glued}$ was 60–90% (Fig. 4A,B), allowing cell viability upon knockdown of this essential protein, which has multiple functions in the cell (Schroer et al., 1996). At these $p150^{glued}$-knockdown conditions, formed cargo carriers appeared considerably smaller when compared to control sample (Fig. 4C; Movies 4 and 5). Quantification of cargo accumulation at ERES showed a 30–60% reduction of cargo concentration in $p150^{glued}$-deficient cells when compared to the control knockdown (Fig. 4D).

Journal of Cell Science (2015) 128, 4160-4170 doi:10.1242/jcs.172395

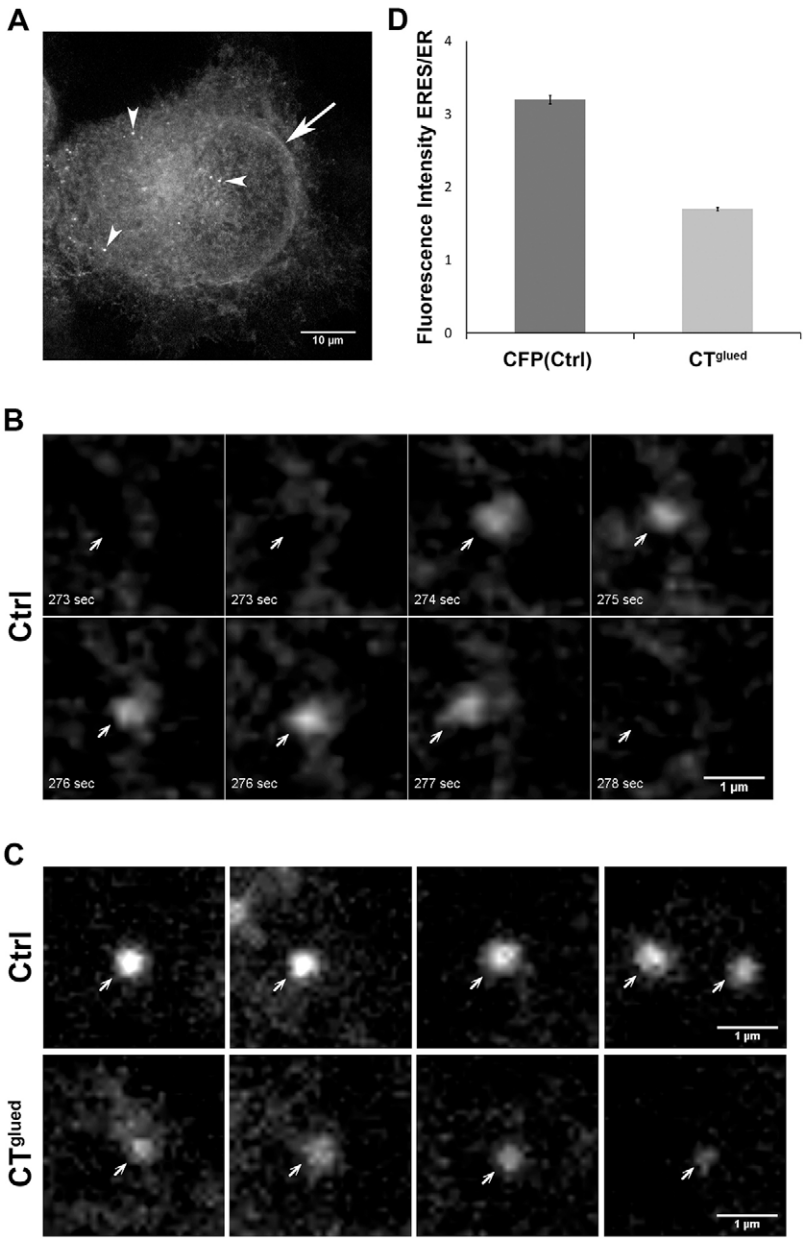

Fig. 3. Expression of CT^{glued} inhibits cargo concentration at ERES. Cells transfected with CFP or CFP-tagged CT^{glued} were infected with adenovirus encoding YFP-tagged ts-O45-G and incubated at 39.5°C for 16 h to accumulate the secretory marker in the ER. Upon shifting to the permissive temperature (32°C) cells were imaged by time-lapse microscopy (see Materials and Methods). (A) Representative image of YFP-tagged ts-O45-G, taken 3 min after the temperature shift. Ts-O45-G is seen in the ER (indicated by a prominent fluorescence of the nuclear envelope, arrow) and in distinct structures (ERES, arrowheads) with increased intensity compared to the surrounding ER (see also Movie 1). (B) Representative timecourse image sequence of ts-O45-G accumulation at single ERES (arrows) and subsequent release of the transport intermediate in a cell transfected with CFP. (C) Example images of ts-O45-G accumulation at different ERES just before release of the transport intermediates in cells transfected with CFP (top panels, labeled Ctrl) and in cells transfected with CFP-tagged CT^{glued} (bottom panels). (D) Accumulation of ts-O45-G at ERES (quantified as described in the Materials and Methods) is seen to be reduced upon expression of CT^{glued}. Mean±s.e.m. for at least 144 ERES in 7 cells per condition are shown.

In addition, the number of ts-O45G carriers observed above the ER upon p150^{glued}-knockdown decreased by 50–70% when compared to control cells (Fig. 4E).

Taken together, results obtained with the antagonist of p150^{glued} and with downregulated levels of the endogenous p150^{glued} clearly support our model prediction that interaction of p150^{glued} with the COPII coat has a role in cargo concentration at ERES.

To determine whether the role of p150^{glued} at ERES depends on the presence of microtubules, we quantified cargo concentration as described with or without the presence of the microtubule-depolymerizing drug nocodazole. The results show a similar degree of cargo concentration in control cells compared to cells treated with nocodazole (control, 3.00±0.09; nocodazole, 2.60±0.05; mean±s.e.m., for each condition $n \geq 9$) (Fig. 5A,B,D). The small apparent reduction in cargo concentration due to nocodazole treatment might be explained by the fact that a lack of microtubules shrinks the spatial extension of the ER network: the local condensation of ER tubules in the absence of microtubules slightly increases the fluorescence intensity in each ER-containing volume element leading to a decrease in the fluorescence ratio for the ERES to ER because of an increased denominator. As expected, in contrast to untreated control cells, the cargo structures forming in the presence of nocodazole did not move towards the Golgi complex (see Movie 3). Instead, they further increased in intensity, consistent with further rounds of COPII carrier formation at the same ERES (Fig. 5B). These data are in agreement with earlier work demonstrating that ER-to-Golgi transport can occur with almost unperturbed kinetics after an extended treatment of cells with nocodazole (Cole et al., 1996), which results in the breakdown of the Golgi complex and a relocation of Golgi mini stacks close to ERES. Our data here is consistent with previous results and suggest that COPII-mediated cargo concentration at ERES does not require the presence of microtubules.

Next, we measured cargo concentration at ERES in cells expressing CT^{glued} with and without nocodazole. As above, a reduction in cargo concentration at ERES was measured in cells

Journal of Cell Science (2015) 128, 4160-4170 doi:10.1242/jcs.172395

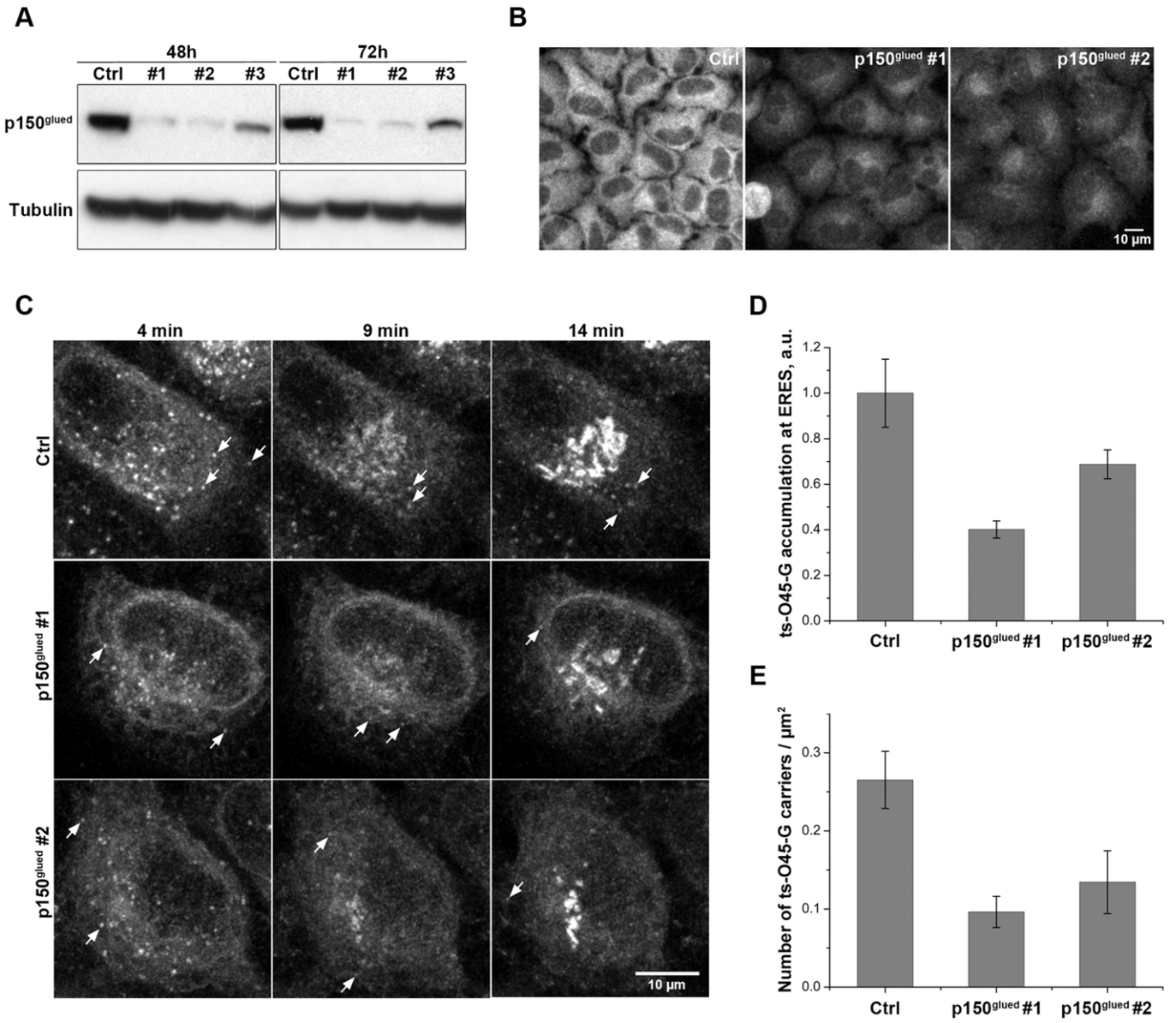

Fig. 4. Knockdown of p150^{glued} inhibits cargo concentration at the ERES. (A) Cells were treated with three different siRNAs against p150^{glued} (#1, #2, and #3) or with control siRNA against LMNA1 (Ctrl). The amount of p150^{glued} was evaluated by western blotting after 48 h or 72 h. Knockdown efficiency of p150^{glued} was ~90% for siRNA #1 and #2, and 75% for siRNA #3. The two most efficient siRNAs were selected for further experiments. (B) The efficiency of p150^{glued} knockdown was also evaluated by immunofluorescence. Relative to the control sample (left) siRNA constructs #1 and #2 (middle and right) decreased the average cell fluorescence intensity by ~60% after 48 h. Average projections of confocal z-stacks are represented. (C) Cells treated with siRNA against p150^{glued} or with a control siRNA against LMNA1 were infected with ts-O45-G–CFP. After 14 h of expression in the ER at 39.5°C, cells were shifted to 32°C and imaged by time-lapse microscopy. Snapshots represent maximum projections of seven confocal slices at 4, 9 and 14 min after the temperature shift. Arrows highlight emerging COPII carriers. In cells treated with siRNA #1 and #2 against p150^{glued} (middle and bottom panels) transport carriers accumulate less cargo as compared to the control (Ctrl, top panels). (D) Time-lapse acquisitions were used to quantify accumulation of ts-O45-G at ERES as described in the Materials and Methods. Treatment of the cells with either siRNA #1 and #2 against p150^{glued} resulted in a decrease by 60% and 31% of cargo accumulation at ERES when compared to the control (Ctrl). Results are mean±s.e.m. for at least for at least 30 cargo carriers per condition. a.u., arbitrary units. (E) The number of ts-O45-G positive structures that are visible above the ER background was quantified 5 min after the temperature shift in control and p150^{glued} siRNA-treated cells. Knockdown of p150^{glued} resulted in a reduction by 50 to 70% of the number of cargo carriers in the cells as compared to the control. Results are mean±s.e.m. for at least 5 cells per condition.

expressing CT^{glued} in the absence or presence of the microtubule-depolymerizing drug (CT^{glued} 1.70±0.05, CT^{glued}+nocodazole 1.65±0.08; compare Figs 3C,D and 5C,D). These results strongly suggest that cargo concentration at ERES does not depend on microtubules, but rather is regulated by p150^{glued} through its interaction with SEC23, which has been shown to also occur in the absence of microtubules (Watson et al., 2005).

DISCUSSION

The earlier observation that p150^{glued}, a component of the dynein-associated dynactin complex, colocalizes with COPII proteins and interacts with SEC23 (Watson et al., 2005) suggested that p150^{glued} might play a regulatory role at ERES. Indeed, expression of the antagonist CT^{glued} had revealed a reduction in the amount of cargo arriving at the Golgi (Watson et al., 2005), yet

Journal of Cell Science (2015) 128, 4160-4170 doi:10.1242/jcs.172395

whether sorting had already failed at the level of ERES had remained elusive. To address this question and to gain insight into the regulation of COPII turnover by p150^{glued}, we quantified the residence times of stably expressed, fluorescently tagged COPII components on single ERES with FRAP. The experimental recovery curves and ERES-bound fractions of COPII components were fed into a mathematical model (Fig. 2) that included individual binding steps for different components of the COPII coat. As a result of combining quantitative microscopy with modeling, we were able to predict that p150^{glued} stabilizes the COPII pre-budding complex in a microtubule-independent manner. In support of this prediction, subsequent experiments revealed a clear reduction of cargo concentration at single ERES upon expression of the antagonist CT^{glued} irrespective of the presence of microtubules.

Despite its attained complexity, our kinetic model might provoke the criticism of being too simple; however, in analogy to an *in vitro* assay all generic reactions are included. Besides, we speculate that with current knowledge, a more-detailed model is unlikely to yield a deeper understanding of the COPII assembly–disassembly mechanism, as a number of parameters that cannot be tested experimentally would lead to a severely underdetermined model. The model we present here balances simplicity and detail by taking into account only the main processes. Moreover, we would like to emphasize that the model cannot make *ab initio* predictions, but its parameters have to be determined by comparing with experimental (FRAP) data.

Our FRAP and modeling data show that p150^{glued} stabilizes the COPII pre-budding complex, most likely by mediating sorting and concentration of cargo, before the binding of SEC13–SEC31. This yields a full, yet rapidly decaying, COPII complex that is capable of finishing COPII vesicle formation. Thus, p150^{glued} supports two subsequent events: (1) cargo selection at ERES and (2) long-range transport of carriers through dynein. As a consequence, p150^{glued} facilitates the anterograde flux along the early secretory pathway by linking the formation and loading of transport carriers to their subsequent transport towards downstream organelles, for example, the Golgi complex.

The COPII pre-budding complex that is stabilized by p150^{glued} is known to be necessary and sufficient to immobilize and capture cargo (Aridor et al., 1998). We therefore speculate that secretory cargo and cargo receptors bound by the premature COPII complex would reside in the ERES area for a longer period, increasing the local concentration of cargo. Several rounds of premature complex assembly and disassembly with concomitant cargo binding might be the molecular mechanism for cargo concentration at ERES. In line with this prediction, Sato and Nakano have proposed that multiple SAR1 hydrolysis cycles could lead to cargo concentration (Sato and Nakano, 2005). Similarly, the formation of abortive clathrin-coated pits is linked to cargo capture (Ehrlich et al., 2004).

Hypothetically, FRAP on ERES could be used to directly test the stabilization of cargo by pre-budding complexes, as predicted by our mathematical model. However, the interpretation of such experiments is likely to be ambiguous: COPII components rapidly diffuse through the cytoplasm and generate a fluorescence recovery only due to association to and dissociation from ERES, whereas cargo molecules (like ts-O45-G) are integral membrane proteins that enter and leave ERES by slow lateral diffusion on ER membranes. Prolonged interaction with pre-budding complexes therefore will be encoded in a reduced diffusion constant of cargo in the ERES region. However, the typical diffusion time for cargo molecules through an ERES is comparable to the residence time of COPII

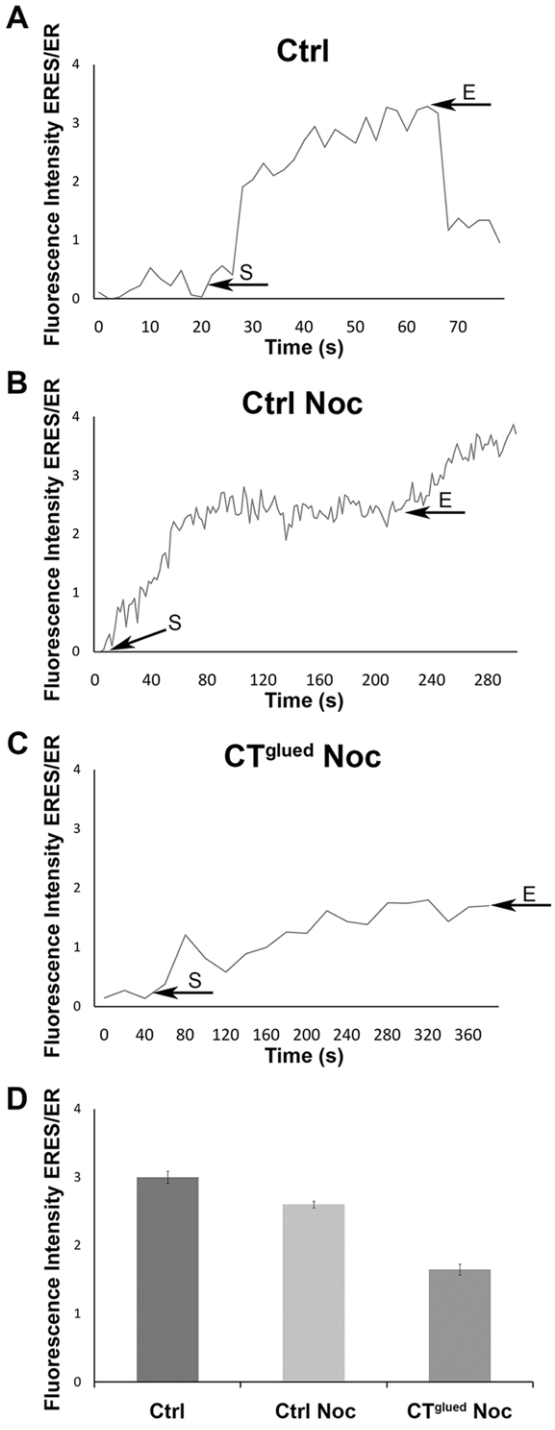

Fig. 5. Cargo accumulation at ERES is independent of microtubules. Cells expressing ts-O45-G–YFP in the ER at 39.5°C were treated with buffer or nocodazole (Noc) for 30 min to depolymerize microtubules. Subsequently the temperature was shifted to 32°C and cells were imaged by time-lapse microscopy and ts-O45-G accumulation in ERES was quantified in each frame and plotted over time (see Materials and Methods for details). Timecourse of ts-O45-G accumulation in (A) control cells, (B) nocodazole-treated cells and (C) CT^{glued}-expressing cells treated with nocodazole. Arrows S and E indicate the average minimum and maximum fluorescence intensities of ts-O45-G at the start and at the end of cargo accumulation cycle, respectively. In nocodazole-treated cells, only the initial cargo concentration at ERES was used for quantification because a second step of cargo concentration starts after E. (D) The accumulation of ts-O45-G at ERES was quantified as described in the Materials and Methods. Mean±s.e.m. for at least nine ERES in four cells are shown.

Journal of Cell Science (2015) 128, 4160-4170 doi:10.1242/jcs.172395

complexes on ERES, and therefore only moderate changes in the diffusion of cargo due to interaction with pre-budding complexes are to be expected. Quantifying diffusion constants by performing FRAP with the required accuracy would be a technical challenge (Weiss, 2004). These substantial uncertainties are further enhanced by the variable sizes and geometries of emerging buds within ERES. Moreover, proper quantification of cargo mobility through FRAP would also be hampered by the presence of cargo-filled carriers that have just pinched off from ERES and cannot be dissected as distinct structures due to the diffraction limit. Unlike cargo-filled buds on ERES, cargo molecules in these topologically distinct structures cannot exchange with the surrounding ER to contribute to the fluorescence recovery.

Consistently, our data suggest that binding of p150^{glued} to SEC23 stabilizes the interaction of SEC23–SEC24 and cargo and might inhibit the recruitment of the SEC13–SEC31 complex allowing cargo concentration and avoiding premature formation of COPII vesicles. It is conceivable that p150^{glued} or other dynactin components might sterically interfere with the very tight and large interaction region of SEC23 and SEC13–SEC31 seen in the structure of the COPII complex (Bi et al., 2007), hence inhibiting the recruitment of SEC13–SEC31 to the pre-budding complex. In the unperturbed scenario, without CT^{glued}, the release of p150^{glued} from SEC23 or conformational changes might liberate sites for SEC13–SEC31 binding and at the same time trigger the capture of a microtubule and the recruitment of a complete dynein–dynactin complex for subsequent transport towards the Golgi complex. A possible protein contributing to this process is TRAPPC9, a component of the transport protein particle (TRAPP) tether complex. This protein binds to the same p150^{glued} domain as SEC23 and inhibits the interaction of SEC23–SEC24 with p150^{glued} disrupting the colocalization of ERES and p150^{glued} (Zong et al., 2012). Indeed, the competition of SEC23 and TRAPPC9 for the same domain of p150^{glued} might be key for the role of p150^{glued} at different stages of ER-to-Golgi transport. For example, when p150^{glued} binds to SEC23 it regulates COPII cargo concentration and vesicle formation, whereas subsequent binding to TRAPPC9 might regulate transport along microtubules towards the cis-Golgi.

We speculate that different splice variants of SEC31 might serve different purposes during the final assembly of COPII complexes and the associated formation of transport intermediates. Contrary to our FRAP results on the stably expressed fluorescently tagged SEC31 variant, previous FRAP data on a SEC31 splice variant yielded a reduced residence time on ERES in the presence of CT^{glued} (Watson et al., 2005). Whereas the latter could in principle reflect a particular behavior due to the transient expression of SEC31, we rather propose that different SEC31 variants might be key for adapting and shaping transport carriers (Stagg et al., 2008) after the pre-budding complex has accomplished its function as a cargo selector. Therefore, ERES residence times specific to each SEC31 splice variant could be possible and meaningful without contradicting the results reported here.

In conclusion, our data provide strong evidence that the previously described SEC23–p150^{glued} interaction stabilizes the COPII pre-budding complex in a microtubule-independent manner. This interaction might provide sufficient time for cargo concentration and transport carrier formation at ERES. This scenario yields a molecular basis for the integration of cargo concentration and COPII transport carrier formation with subsequent transport i.e. SAR1A and SEC31A to the Golgi complex along microtubules.

MATERIALS AND METHODS

Materials

Cycloheximide was from Calbiochem. Plasmids encoding YFP–SEC23A, YFP–SAR1A and YFP–SEC31A are as described previously (Forster et al., 2006; Runz et al., 2006). CT^{glued} was a gift from David Stephens (University of Bristol, UK). ts-O45-G–YFP and ts-O45-G–CFP were obtained from Kai Simons (MPI-CBG, Dresden, Germany). Polyclonal anti-SEC23 antibody was a gift from Chris Fromme and Randy Schekman or from Abcam, monoclonal anti-SEC31 antibody was from BD Biosciences, polyclonal anti-SAR1 antibody was from Upstate, monoclonal anti-GFP antibody was from Roche, monoclonal anti-tubulin antibody was from Neomarkers, Rabbit polyclonal anti-SEC13 antibody was raised and purified against recombinant human SEC13. Scramble, SEC31L1, SEC31L2, p150^{glued} and LMNA1 siRNAs were from Ambion.

Cell culture

HeLa-Kyoto (human cervix carcinoma cells), a gift from Shuh Narumiya, (Kyoto University, Japan) and Toru Hirota (IMP Vienna, Austria), were grown in Dulbecco's modified Eagle's medium (DMEM; Life Technologies, Karlsruhe, Germany) supplemented with 10% fetal bovine serum (FBS), 1% penicillin and streptomycin and 1% glutamine in a 37°C humidified incubator containing 5% CO_2. Transient transfections were performed following the manufacturer's recommendations using FuGENE® 6 Transfection Reagent (Roche, Applied Science). Transfection efficiency for CT^{glued} was 5–10%, resulting in low and constant expression levels of the protein. siRNAs were transfected with lipofectamine RNAiMAX (Invitrogen) transfection reagent according to the manufacturer's instructions. For live-cell imaging or immunostaining cells were grown on live-cell dishes (MatTEk, Ashland, MA or Lab-Tek II Chambered coverglass, Nunc) or 15-mm coverslips for experiments with fixed cells.

Generation and characterization of stable cell lines

HeLa Kyoto cells were transfected as described above. Selection of stable clones expressing YFP–SEC23, YFP–SEC31 or YFP–SAR1 was performed in the presence of 500 µg/ml of G418 (Life Technologies Inc.). After G418 selection, one to four YFP-expressing cells were sorted into single wells of 96-well plates by flow cytometry using a DAKO MoFlo with an excitation at 488 nm and 80 mW and cultivated until confluency was reached. Thereafter, another two rounds of sorting by flow cytometry and subsequent clone expansion were performed.

In these cell lines, the YFP-tagged SAR1, SEC23 or SEC31 colocalized extensively with endogenous SEC31 (see Fig. 1). No apparent difference in the distribution of cytoplasmic organelles and structures (e.g. Golgi, ER or microtubules) between the parental cell lines and those expressing YFP-tagged COPII components was found (data not shown). Kinetics of ts-O45-G transport from the ER to the plasma membrane was similar between the parental cell line and those expressing YFP-tagged COPII components. However, in the YFP–SEC31 cell line ~10% of the cells showed significantly elevated levels of YFP–SEC31. Because in these cells ts-O45-G transport to the plasma membrane was inhibited, we excluded cells with extremely high YFP levels from our experiments. Immunoprecipitation of YFP-tagged COPII components followed by analysis of the precipitates by western blotting or mass spectrometry showed that all YFP-tagged COPII components interact with endogenous COPII components (data not shown). Cell lines with distinct levels of expression did not show different recovery kinetics.

Immunostaining

HeLa Kyoto cells were fixed either with 100% methanol at −20°C for 4 min or with 3% paraformaldehyde (PFA) for 20 min at room temperature. PFA-treated cells were subsequently treated with 30 mM glycine in PBS for 5 min and subsequently permeabilized with 0.1% Triton X-100 in PBS for a further 5 min. Fixed and permeabilized cells were incubated with primary antibodies in PBS for 30 min. Samples were then washed three times for 5 min in PBS and incubated for 20 min in Alexa-Fluor-568-conjugated anti-rabbit-IgG or anti-mouse-IgG secondary antibodies, and finally washed three times for 5 min in PBS. Cells grown

Journal of Cell Science (2015) 128, 4160-4170 doi:10.1242/jcs.172395

on coverslips were mounted on glass slides with Mowiol. Cells grown in live-cell dishes were left in PBS.

FRAP experiments and quantification of the steady-state ERES-bound fraction of YFP-tagged COPII subunits

Hela Kyoto cells were imaged and photobleached at 37°C in carbonate-free imaging medium using an SP2 laser scanning confocal microscope (Leica) as previously described (Forster et al., 2006; Runz et al., 2006). In all experiments, single ERES were bleached, representing ∼0.1% of the total cell area. Bleaching of YFP was adjusted such that ∼50% of the prebleach fluorescence was irreversibly bleached. Data analysis was performed as described previously (Forster et al., 2006; Runz et al., 2006). In each photobleaching experiment images of the living cells after the photobleaching were used to determine the ratio of total fluorescence associated with ERES and total cellular fluorescence (named the 'ERES-bound steady-state protein fraction'; Forster et al., 2006 and Runz et al., 2006, for details). These fractions did not appear to depend on the amount of YFP-tagged COPII subunits expressed.

Quantifying the concentration of ts-O45-G at ERES

To study the effect of CT^{glued} and microtubules on cargo concentration at individual ERES, cells were transfected with siRNA for 48 h or co-transfected with plasmids encoding either CFP or CFP–CT^{glued} and ts-O45-G–YFP and incubated at 39.5°C for 16 h. Thereafter, they were either treated with buffer or 10 mM nocodazole for 30 min at 39.5°C before being transferred into pre-warmed (32°C) imaging medium and moved directly onto a Perkin Elmer Ultraview ERS spinning disk confocal microscope equilibrated at 32°C. Immunostaining of nocodazole-treated cells against tubulin did not reveal detectable levels of intact microtubules. For each cell, three-dimensional stacks of eight to ten different image planes were acquired every 2, 7 or 20 s for a total period of 5–20 min. These stacks were subjected to maximum projections using ImageJ and QuickTime movies of the maximum projections were generated.

To quantify the concentration of ts-O45-G–YFP at ERES in buffer- or nocodazole-treated cells, the fluorescence intensities of ts-O45-G at single ERES and neighboring reticular ER membranes were quantified in each frame. Cell background fluorescence was subtracted from the intensity at ERES and reticular ER and the ratio (ERES:ER) plotted over time. The concentration of ts-O45-G at ERES was calculated by subtracting the minimum ratio ('S' for the start of cargo accumulation; see Fig. 5A–C) from the maximum ratio ('E' for the end of cargo accumulation; see Fig. 5A–C) obtained. If ratios showed fluctuations around an average value for several time-points, these average values were used to determine 'S' or 'E'. At least nine ERES from four different cells (in total at least 18 concentration steps) were quantified for both nocodazole-treated and control cells.

For quantifying ts-O45-G concentrations in CFP- or CFP-CT^{glued}-expressing cells (Fig. 3) fluorescence ratios (ERES:ER) were only determined for time-points just before the release of a ts-O45-G-loaded carrier from the ERES and its subsequent motion towards the Golgi complex. Usually this represents the highest ERES:ER ratio obtained for one carrier release from the ERES. For these experiments, we quantified, in each case, at least 15 vesicular tubular clusters (VTCs) from seven different cells from cells transfected with either CFP or CFP-tagged CT^{glued}.

To quantify the concentration of secretory cargo at ERES upon knockdown of $p150^{glued}$, cells were transfected with control or siRNA against $p150^{glued}$. After 48 h, cells were infected with recombinant adenovirus encoding ts-O45-G–CFP and incubated at 39.5°C for 14 h. Thereafter, cells were transferred into pre-warmed (32°C) imaging medium and moved directly onto a Zeiss LSM780 laser scanning confocal microscope equilibrated at 32°C. For each cell, three-dimensional stacks of seven image planes were acquired every 5 s for a total period of 10 min starting 4 min after the temperature shift. Images were subjected to low-pass filtering to reduce the noise and movies of maximum projections of the acquired stacks were generated. Image background fluorescence was subtracted from projected images, which were then used to identify cargo-loaded carriers. Masks corresponding to the tracked carrier and neighboring ER region were defined and fluorescence intensities were quantified in the last frame before the carrier moved towards the Golgi complex. Cargo accumulation at ERES was quantified as the integrated intensity of the carrier normalized to the mean intensity of the neighboring ER region. For each condition at least 30 cargo carriers from five different cells were quantified.

To quantify the effect of $p150^{glued}$ knockdown on the number of ts-O45-G-positive cargo carriers, images at 5 min after the temperature shift were used. First, cells were segmented manually and ts-O45-G carriers were segmented with a constant threshold level after subtracting local background from each pixel of the image. This background was generated by applying sequentially minimum and maximum filters on the original image (method known as top-hat transformation). The number of identified structures was then divided by the area of the cell. A minimum of five cells was analyzed for each condition.

Kinetic model

To mathematically formulate the model sketched in Fig. 2A, we first employed the law of mass action to obtain a set of ordinary differential equations (ODEs) for the concentrations of membrane-bound protein complexes (denoted by square brackets):

$$\frac{d}{dt}[S_m] = k'[S_c] - \Gamma[S_m] - \omega'[S_m][C_c]$$

$$\frac{d}{dt}[C_m] = \omega'[S_m][C_c] - \gamma_1[C_m] - \beta'[C_m][K_c]$$

$$\frac{d}{dt}[C^*] = \gamma_1[C_m] - \lambda_1[C^*]$$

$$\frac{d}{dt}[K_m] = \beta'[C_m][K_c] - \gamma_2[K_m]$$

$$\frac{d}{dt}[K^*] = \gamma_2[K_m] - \lambda_2[K^*].$$

Here, cytosolic SAR1-GDP, SEC23–SEC24 and SEC13–SEC31, are denoted by $[S_c]$, $[C_c]$, and $[K_c]$, membrane-bound SAR1, and pre-budding complexes with and without SAR1 are indicated by $[S_m]$, $[C_m]$, and [C*], respectively; mature COPII complexes with and without SAR1 are denoted by $[K_m]$, and [K*]. The total (tot) number of proteins of each species is conserved during the experiments, that is, the following particle number conservation laws hold:

$$\begin{aligned} \text{SAR1} \quad & S_{tot} = V[S_c] + A([S_m] + [C_m] + [K_m]) \\ \text{SEC23–SEC24} \quad & C_{tot} = V[C_c] + A([C_m] + [C^*] + [K_m] + [K^*]) \\ \text{SEC13–SEC31} \quad & K_{tot} = V[K_c] + A([K_m] + [K^*]). \end{aligned}$$

Here, the cytosolic volume is denoted by V and A is the effective volume of all ERES in the cell.

Given that FRAP measures the total fluorescence of a protein species, that is, the number of particles rather than the concentration, the set of ODEs needs to be translated to particle numbers. Inserting the above conservation laws into the ODEs and using $s=S_m/S_{tot}$, $c=C_m/C_{tot}$, $b=C^*/C_{tot}$, $a=K_m/K_{tot}$, $e=K^*/K_{tot}$, $R_1=C_{tot}/S_{tot}$, $R_2=K_{tot}/S_{tot}$, $\omega=\omega' S_{tot}/V$, $\beta=\beta' K_{tot}/V$, $k'=kA/V$ yields a set of ODEs that describe our FRAP experiments:

$$\frac{ds}{dt} = k(1 - s - R_1 c - R_2 a) - \Gamma s - s\omega R_1\left(1 - c - b - \frac{R_2}{R_1}(a + e)\right), \quad (1)$$

$$\frac{dc}{dt} = s\omega\left(1 - c - b - \frac{R_2}{R_1}(a + e)\right) - \gamma_1 c - \beta c(1 - a - e), \quad (2)$$

$$\frac{db}{dt} = \gamma_1 c - \lambda_1 b, \quad (3)$$

$$\frac{da}{dt} = \beta c\frac{R_1}{R_2}(1 - a - e) - \gamma_2 a, \quad (4)$$

$$\frac{de}{dt} = \gamma_2 a - \lambda_2 e. \quad (5)$$

The total fluorescence of ERES-bound COPII proteins (normalized to the total pool of the respective protein species) is hence $F_{SAR1}(t)=s+R_1c+R_2a$,

$F_{SEC23}(t) = c + b + \frac{R_2}{R_1}(a + e)$ and $F_{SEC31}(t)$=a+e. These values can be compared directly to the ERES-bound steady-state fraction of COPII proteins determined through fluorescence imaging by calculating the steady-state (a_0, b_0, c_0, e_0, s_0) of Eqns 1–5 for parameter sets (R_1, R_2, k, Γ, ω, β, γ_1, γ_2, λ_1, λ_2). From this, the steady-state fraction of SEC23–SEC24 in pre-budding complexes that never recruit SEC13–SEC31 is simply determined as:

$$\frac{\text{SEC23}-\text{SEC24}_{\text{pre}}}{\text{SEC23}-\text{SEC24}_{\text{tot}}} = \frac{p[C_m] + [C^*]}{[C_m] + [C^*] + [K_m] + [K^*]} = \frac{pc_0 + b_0}{c_0 + b_0 + R_2(a_0 + e_0)/R_1}.$$

Here, concentrations of SEC23–SEC24 have been expressed in terms of scaled quantities considered in Eqns 1–5, and the prefactor p determines the fraction of SAR1–SEC23–SEC24 complexes that follow the disassembly route rather than recruiting SEC13–SEC31. This fraction can be calculated easily by considering only the losses from state C_m (=c in scaled units) at steady state:

$$\mathrm{p} = \frac{\gamma_1 c_0}{\gamma_1 c_0 + \beta(1 - a_0 - e_0)}.$$

If a randomly chosen parameter set yielded steady states that were consistent with our experimental data, FRAP experiments were simulated with Eqns 1–5 for these parameters: in accordance with the experiment, photobleaching was assumed to reduce the fluorescent species of interest to 50% of its steady-state signal, while all other species were left unaffected in the steady state. Recovery curves were calculated for a total time of 30 s by an Euler forward differencing method (Press et al., 1992) using a time increment of Δt=0.5 ms. Simulated FRAP curves were fitted with a single exponential recovery like the experimental data. Only those parameter sets for which the calculated recovery times and steady states matched the mean values of Table 1 within one standard deviation were stored for further analysis. In total $\sim 10^9$ parameter sets were screened for each experimental condition (with or without CT^{glued}), which resulted in 2000 valid parameter sets for each, untreated and CT^{glued}-expressing cells. Normalized distribution functions (histograms) of these parameters were calculated on logarithmic scales to cover the screened parameter ranges. Using these histograms, the overlap area between parameters found for untreated and CT^{glued}-expressing cells were calculated by numerical integration (gray-shaded regions in Fig. 2B). Table 2 reports geometric averages of the respective values for the parameters found in the numerical screen. A geometric average was chosen to properly consider the logarithmic fluctuations of parameters.

During the screen, parameters were chosen randomly (equidistributed on a logarithmic scale) in the following ranges: R_1, $R_2 \in [0.1, 2]$, γ_1, γ_2, λ_1, $\lambda_2 \in [0.1/s, 10/s]$, $\Gamma \in [0.01/s, 1000/s]$, and k, ω, $\beta \in [0.001/s, 1000/s]$. These intervals were been picked because the expression ratios of COPII proteins are known to vary by at most tenfold (Wisniewski et al., 2012), and simple off-rates need to lie roughly in the range of the observed inverse FRAP times (Hoffmann et al., 2015). Rates that have been defined in a more complex way were screened over a wider range to not miss valid parameter sets.

Acknowledgements
We are grateful to K. Simons, D. Stephens, C. Fromme and R. Schekman for gifts of reagents and M. Kaksonen and Camilla Godlee for critical reading of the manuscript. We also thank B. Joggerst and the EMBL ALMF team for their continuous help during the project. The support of the ALMF at EMBL by Perkin Elmer, Leica Microsystems, Olympus Europe and Carl Zeiss is acknowledged. We are grateful to A. Riddle from the Flow Cytometry Core Facility at EMBL for his support in handling and sorting cells by FACS and K. Miura for providing macros for FRAP data and ts-O45-G quantification.

Competing interests
The authors declare no competing or financial interests.

Author contributions
F.V. designed and performed experiments, acquired and analyzed data; A.H. acquired and analyzed data; R.P. designed experiment and mathematical model; M.W. designed and elaborated mathematical model. All authors wrote the manuscript.

Funding
F.V. was funded by the Fundação para a Ciência e Tecnologia fellowship [grant number SFRH/BPD/22014/2005]. M.W. acknowledges support by the Deutsche Forschungsgemeinschaft (DFG) [grant number WE4335/2-1 and HFSP grant RGY0076/2010]. A.H. was funded by the Center for Modelling and Simulation in the BioSciences (BIOMS, Heidelberg, Germany).

Supplementary information
Supplementary information available online at
http://jcs.biologists.org/lookup/suppl/doi:10.1242/jcs.172395/-/DC1

References
Antonny, B., Madden, D., Hamamoto, S., Orci, L. and Schekman, R. (2001). Dynamics of the COPII coat with GTP and stable analogues. *Nat. Cell Biol.* **3**, 531-537.
Aridor, M., Weissman, J., Bannykh, S., Nuoffer, C. and Balch, W. (1998). Cargo selection by the COPII budding machinery during export from the ER. *J. Cell Biol.* **141**, 61-70.
Barkai, N. and Leibler, S. (1997). Robustness in simple biochemical networks. *Nature* **387**, 913-917.
Barlowe, C. (2002). COPII-dependent transport from the endoplasmic reticulum. *Curr. Opin. Cell Biol.* **14**, 417-422.
Bi, X., Mancias, J. D. and Goldberg, J. (2007). Insights into COPII coat nucleation from the structure of Sec23·Sar1 complexed with the active fragment of Sec31. *Dev. Cell* **13**, 635-645.
Cole, N. B., Sciaky, N., Marotta, A., Song, J. and Lippincott-Schwartz, J. (1996). Golgi dispersal during microtubule disruption: regeneration of Golgi stacks at peripheral endoplasmic reticulum exit sites. *Mol. Biol. Cell* **7**, 631-650.
Culver-Hanlon, T. L., Lex, S. A., Stephens, A. D., Quintyne, N. J. and King, S. J. (2006). A microtubule-binding domain in dynactin increases dynein processivity by skating along microtubules. *Nat. Cell Biol.* **8**, 264-270.
Ehrlich, M., Boll, W., Van Oijen, A., Hariharan, R., Chandran, K., Nibert, M. L. and Kirchhausen, T. (2004). Endocytosis by random initiation and stabilization of clathrin-coated pits. *Cell* **118**, 591-605.
Forster, R., Weiss, M., Zimmermann, T., Reynaud, E. G., Verissimo, F., Stephens, D. J. and Pepperkok, R. (2006). Secretory cargo regulates the turnover of COPII subunits at single ER exit sites. *Curr. Biol.* **16**, 173-179.
Hehnly, H. and Stamnes, M. (2007). Regulating cytoskeleton-based vesicle motility. *FEBS Lett.* **581**, 2112-2118.
Hoffmann, J., Fickentscher, R. and Weiss, M. (2015). Influence of organelle geometry on the apparent binding kinetics of peripheral membrane proteins. *Phys. Rev. E* **91**, 022721.
King, S. J. and Schroer, T. A. (2000). Dynactin increases the processivity of the cytoplasmic dynein motor. *Nat. Cell Biol.* **2**, 20-24.
Lee, M. C. S., Miller, E. A., Goldberg, J., Orci, L. and Schekman, R. (2004). Bi-directional protein transport between the ER and Golgi. *Annu. Rev. Cell Dev. Biol.* **20**, 87-123.
Matsuoka, K., Orci, L., Amherdt, M., Bednarek, S. Y., Hamamoto, S., Schekman, R. and Yeung, T. (1998). COPII-coated vesicle formation reconstituted with purified coat proteins and chemically defined liposomes. *Cell* **93**, 263-275.
Otte, S. and Barlowe, C. (2004). Sorting signals can direct receptor-mediated export of soluble proteins into COPII vesicles. *Nat. Cell Biol.* **6**, 1189-1194.
Palmer, K. J., Konkel, J. E. and Stephens, D. J. (2005). PCTAIRE protein kinases interact directly with the COPII complex and modulate secretory cargo transport. *J. Cell Sci.* **118**, 3839-3847.
Presley, J., Cole, N., Schroer, T., Hirschberg, K., Zaal, K. and Lippincott-Schwartz, J. (1997). ER-to-Golgi transport visualized in living cells. *Nature* **389**, 81-85.
Press, W. H., Teukolsky, S. A., Vetterling, W. T. and Flannery, B. P. (1992). *Numerical Recipes in Fortran 77*. Cambridge University Press, Cambridge UK.
Rismanchi, N., Puertollano, R. and Blackstone, C. (2009). STAM adaptor proteins interact with COPII complexes and function in ER-to-Golgi trafficking. *Traffic* **10**, 201-217.
Runz, H., Miura, K., Weiss, M. and Pepperkok, R. (2006). Sterols regulate ER-export dynamics of secretory cargo protein ts-O45-G. *EMBO J.* **25**, 2953-2965.
Sato, K. and Nakano, A. (2005). Dissection of COPII subunit-cargo assembly and disassembly kinetics during Sar1p-GTP hydrolysis. *Nat. Struct. Mol. Biol.* **12**, 167-174.
Scales, S. J., Pepperkok, R. and Kreis, T. E. (1997). Visualization of ER-to-Golgi transport in living cells reveals a sequential mode of action for COPII and COPI. *Cell* **90**, 1137-1148.
Schroer, T. A., Bingham, J. B. and Gill, S. R. (1996). Actin-related protein 1 and cytoplasmic dynein-based motility - what's the connection? *Trends Cell Biol.* **6**, 212-215.

Slepnev, V. I. and De Camilli, P. (2000). Accessory factors in clathrin-dependent synaptic vesicle endocytosis. *Nat. Rev. Neurosci.* **1**, 161-172.

Stagg, S. M., LaPointe, P., Razvi, A., Gürkan, C., Potter, C. S., Carragher, B. and Balch, W. E. (2008). Structural basis for cargo regulation of COPII coat assembly. *Cell* **134**, 474-484.

Waterman-Storer, C. M., Karki, S. and Holzbaur, E. L. (1995). The p150Glued component of the dynactin complex binds to both microtubules and the actin-related protein centractin (Arp-1). *Proc. Natl. Acad. Sci. USA* **92**, 1634-1638.

Watson, P., Forster, R., Palmer, K. J., Pepperkok, R. and Stephens, D. J. (2005). Coupling of ER exit to microtubules through direct interaction of COPII with dynactin. *Nat. Cell Biol.* **7**, 48-55.

Weiss, M. (2004). Challenges and artifacts in quantitative photobleaching experiments. *Traffic* **5**, 662-671.

Wisniewski, J. R., Ostasiewicz, P., Dus, K., Zielinska, D. F., Gnad, F. and Mann, M. (2012). Extensive quantitative remodeling of the proteome between normal colon tissue and adenocarcinoma. *Mol. Syst. Biol.* **8**, 611.

Zilberstein, A., Snider, M. D., Porter, M. and Lodish, H. F. (1980). Mutants of vesicular stomatitis virus blocked at different stages in maturation of the viral glycoprotein. *Cell* **21**, 417-427.

Zong, M., Satoh, A., Yu, M. K., Siu, K. Y., Ng, W. Y., Chan, H. C., Tanner, J. A. and Yu, S. (2012). TRAPPC9 mediates the interaction between p150 and COPII vesicles at the target membrane. *PLoS ONE* **7**, e29995.